

Feedback Resonating Control For a Wave Energy Converter

Giorgio Bacelli, *Member, IEEE*, Victor Nevarez, Ryan G. Coe, David Wilson, *Member, IEEE*

Abstract—Through the use of advanced control techniques, wave energy converters can achieve substantial increases in energy absorption. The motion of the WEC device is a significant contribution to the energy absorbed by the device. Reactive (“complex conjugate”) control maximizes the energy absorption due to the impedance matching. The issue with complex conjugate control is that, in general, the controller is non-causal, which requires prediction of the incoming waves. This paper explores the potential of employing system identification techniques to build a causal transfer function that approximates the complex conjugate controller over a finite frequency band of interest. This approach is quite viable given the band-limited nature of ocean waves. The resulting controller is stable, and the average efficiency of the power captured by the causal controller in realistic ocean waves is 99%, when compared to the non-causal complex conjugate.

I. INTRODUCTION

Wave energy converters (WECs) interact with and absorb the natural energy in water waves. The nature of this wave-body interaction affects how much of the mechanical energy from the wave is absorbed by the device. Moreover, the interaction is governed by the full system dynamics, which include the input from the generator as well as the wave-body interaction. A simple linear damping control scheme (also known as “passive control”) is simpler to implement, but it provides poor absorption efficiency outside the natural resonance of the wave-body system. As such, a more sophisticated controller is necessary to improve the energy captured by broadening system resonance. The underlying theory for maximum power absorption is well summarized by [1], and is discussed further in Section II. Using this analytical derivation, there have been many control theory implementations to the heave-only oscillating model [2]–[5]. Optimal control analysis of WEC devices are not limited to single body devices and have been expanded to two-body coupled WECs [6]–[8] as well as oscillating water columns (OWCs) [9], [10] and other devices [11], [12].

For this paper, the model-scale experimental WEC device shown in Fig. 1 is considered. This device, which has a major

The authors are with Sandia National Laboratories, Albuquerque, NM, 87123 USA e-mail: gbacell@sandia.gov.

This work was funded by the U.S. Department of Energy’s Water Power Technologies Office. Sandia National Laboratories is a multi-mission laboratory managed and operated by National Technology and Engineering Solutions of Sandia, LLC, a wholly owned subsidiary of Honeywell International, Inc., for the U.S. Department of Energy’s National Nuclear Security Administration under contract DE-NA0003525. This paper describes objective technical results and analysis. Any subjective views or opinions that might be expressed in the paper do not necessarily represent the views of the U.S. Department of Energy or the United States Government.

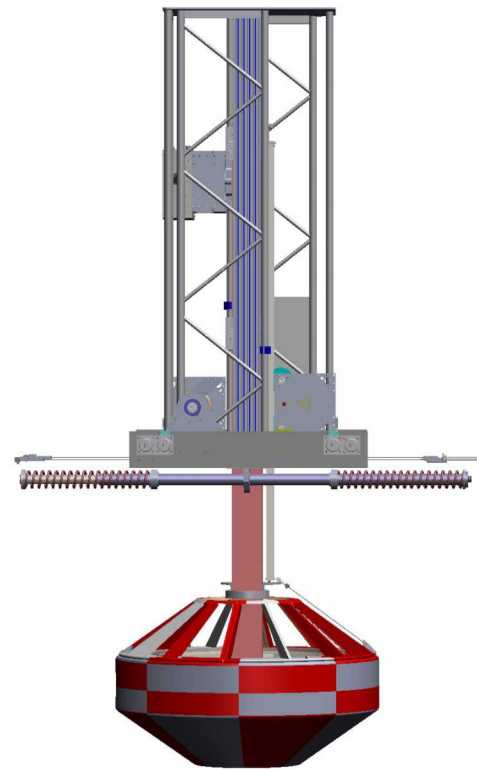


Fig. 1. CAD rendering of “WaveBot” device considered herein.

diameter of 1.76 m, a draft of 0.53 m, and displaces roughly 880 kg of water, was tested at the US Navy’s Maneuvering and Sea Keeping (MASK) basin [13]. For the purposes of this paper specifically, open-loop testing of this so-called “WaveBot” was conducted for system identification (SID). The numerical model of the WEC produced by that process forms the basis for control design considered in this paper.

A. Reactive Control

Two popular strategies for maximum power adsorption that fall under the category of reactive control are phase/amplitude control and complex conjugate control. Phase/amplitude control consists in controlling the velocity of the device so as to follow a prescribed reference that depends on the wave excitation forces and on the model of the device. With complex conjugate control, or impedance matching, the controller matches the impedance to the admittance of the device to allow for maximum energy absorption. The issue

with such an approach is that the impedance matching requires the complex-conjugate of the impedance, which makes the controller acausal. There have been papers on the effects of irregular waves on reactive control [14], [15], as well as signal processing techniques that have been applied to mitigate the anti-causality by improving irregular wave measurements [16]. Due to the acausality of reactive control, future knowledge of the excitation force and incoming wave needs to be known. The sensitivity and requirements for the prediction for reactive have been well studied [16]–[19]. There have even been reactive controller designs where the controller is tuned to the peak frequency of the wave spectrum [14], [15].

In this paper, we are interested in implementing a causal controller using the principle of impedance matching. There have been other various implementations to improve upon the reactive controller, such as using reinforced learning and neural networks [20], [21]. In [22], a causal stochastic optimal control has been implemented on a heaving point absorber. The causal controller was derived by approximating the non-causal control law, which was expressed in terms of a frequency-dependent coefficient proportional to the body velocity and the radiation force. This paper instead focuses on using SID to approximate the non-causal controller with a stable and causal controller, and builds upon the findings presented in [23]. In particular, the controller is a linear time-invariant transfer function, which is considerably easier to derive and implement on a real system, when compared to the other implementations presented in the literature.

B. Paper Outline

This paper is divided in four sections. The analytical formalization and reactive control theory are in Section II, in which the formulation for maximum power capture of a device is derived along with the reactive control law. At the end of Section II, the use of SID is considered to approximate the complex controller. The implementation, stability analysis, and simulation results for both regular and irregular wave input is discussed in Section III. Section IV includes a discussion on how to derive and tune the controller when the dynamics of the power take-off (PTO) cannot be neglected; in particular, when the objective of the control design is to maximize electrical power out of the generator, rather than the mechanical power. Finally, Section V reviews the results and discusses the limitations and improvements of using SID techniques to model a causal reactive controller.

II. CONTROLLER DESIGN

A. Optimal WEC control

The general (loss-free) structure for energy transfer for the WEC device is that the incoming waves produce a force on the body, denoted as F_e , while the body responds with a velocity V and radiates a wave back into the environment; the force acting on the oscillating body due to the radiation is denoted as F_{rad} . The force on the WEC is then transferred onto the PTO, denoted as F_{pto} . In general, the equations of motion are defined as the following:

$$\left(i\omega M + B + \frac{S}{i\omega}\right) V = F_e + F_{rad} + F_{pto}. \quad (1)$$

Here, ω is the angular frequency, M is the mass matrix of the device, B is a damping term describing linear losses and S is the hydro-static restoring coefficient. The radiation force, in turn, is function of the body velocity and it is defined as:

$$F_{rad} = -(i\omega m(\omega) + R(\omega)) V, \quad (2)$$

where $R(\omega)$ and $m(\omega)$ are, respectively, the frequency dependent radiation damping and the added mass.

The mechanical power absorbed by the oscillating body is defined as

$$W_{PTO} = -\frac{1}{2\pi} \int_0^\infty [F_{pto} v^*(\omega) + F_{pto}^*(\omega) v(\omega)] d\omega. \quad (3)$$

From the equation of motion in (1), the intrinsic impedance of the system is defined as the following:

$$Z_i(\omega) = i\omega(M + m(\omega)) + B + R(\omega) + \frac{S}{i\omega}, \quad (4)$$

By using the definition in (4), we see that when the PTO force satisfies

$$F_{pto} = -Z_i^*(\omega) V, \quad (5)$$

then (3) becomes

$$W_{pto,MAX} = \frac{1}{2\pi} \int_0^\infty \frac{|F_e(\omega)|^2}{2R_i(\omega)} d\omega, \quad (6)$$

where R_i is the intrinsic resistance of the device, that is $R_i = \text{Re}[Z_i]$. Consequently, it can be seen that the optimal velocity corresponding to the maximum energy is $v(\omega) = \frac{F_e(\omega)}{2R_i(\omega)}$. From (5) the origin of the terms ‘‘complex conjugate’’ control or ‘‘impedance matching’’ control become evident. Maximum power absorption happens when the PTO impedance matches the complex conjugate of the mechanical impedance of the device, or when the reactance of the PTO cancels the reactance of the device and the resistance of the PTO is equal to the resistance of the device.

As our analysis will be conducted with simulations at specific frequencies, (6) can be simplified to the following equation, which is valid for a sinusoidal excitation:

$$W_{pto,MAX} = \frac{|F_e(\omega_0)|^2}{8R_i(\omega_0)}, \quad (7)$$

where ω_0 is the specific frequency of the excitation force F_e . By looking at the impulse response of the mechanical impedance we get the following response:

$$h_i(t) = K(t) + B\sqrt{2\pi}\delta(t) - M\sqrt{2\pi}\delta(t) - S\sqrt{\frac{\pi}{2}}\text{sgn}(t), \quad (8)$$

where K is the causal impulse response of the radiation impedance [2] and $\delta(t)$ is the Dirac delta. Here we can see that the last term in (8) is the non-causal term where $h_i(t) = S\sqrt{\frac{\pi}{2}}$ for $t < 0$.

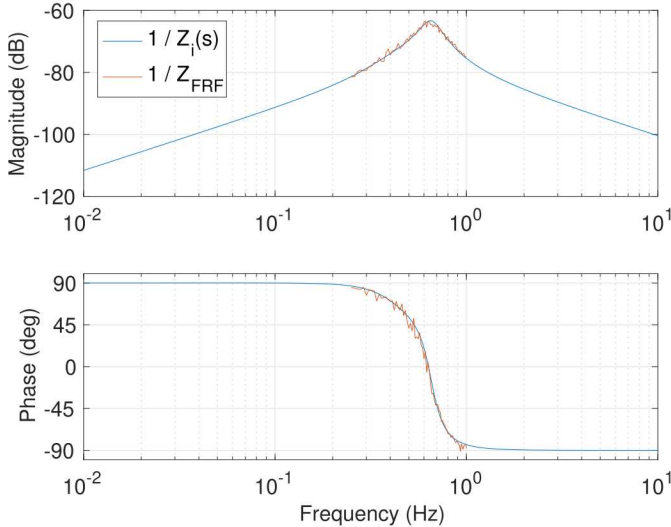


Fig. 2. Bode plots of the plant model in both parametric form (blue line) and non-parametric form (red line).

B. Controller Design

SID methods are used in several engineering fields to produce models of various dynamic systems from measured data. Fundamentally, SID techniques rely upon characterizing a system based on how the system's output responds to various inputs. Input signals are important, as they affect the quality of output response. In other words, if the dynamics of the system are not fully explored, the SID model will not properly model the system. Thus, when designing an experiment for SID, it is important to consider a number of factors, such as signal bandwidth, improvement of model quality, cost of the experiment, and increased noise sensitivity.

SID techniques have been used to characterize WEC devices using various models and approaches [24]–[26]. These modeling approaches can be characterized as one of the following: white box (with model formulation), grey box (basic physical understanding of system), and black box (no knowledge of the system). Typically, for wave energy, there is some knowledge of the system (e.g., stiffness and mass from geometric measurements), thus SID techniques use grey box modeling. Using the built-in SID toolboxes in MATLAB, and by assuming that the hydrostatic coefficient S and the mass M are known with good accuracy, a grey box model can be used to determine the WEC intrinsic impedance by using the model in (1) (comprehensive details on this procedure can be found in [24]).

According to (5), the optimal feedback law is the complex conjugate of the impedance Z_i ; however, Z_i is stable and causal, therefore the complex conjugate of Z_i is non-causal. The approach studied in this paper is to approximate the non-causal optimal feedback with a causal linear time-invariant controller. The approximation is carried out by using SID over a limited frequency band; this is due to the well known Bode-Fano limit [27] [28], which states that impedance matching can only be achieved over a finite frequency range. More precisely, there is always a trade-off between the accuracy of the impedance matching approximation and the bandwidth

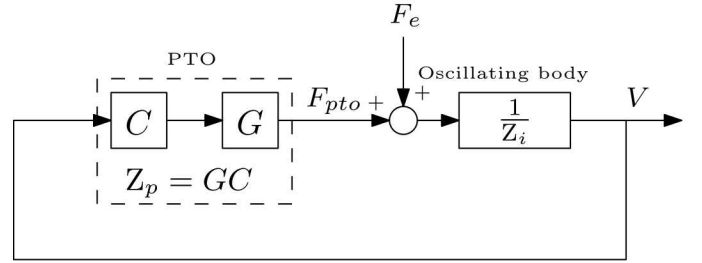


Fig. 3. System block diagram for reactive control for WEC.

over which the approximation is carried out.

The Bode diagram of the WaveBot intrinsic impedance is shown in Fig. 2; where the experimental setup and data analysis are thoroughly described in [24]. For the case considered in this paper, the intrinsic impedance is obtained using a multisine input with frequency range $0.25 \leq f \leq 1$ Hz. In particular, the red curve denotes the non-parametric model and the blue curve is the estimated parametric model obtained using SID.

MATLAB's System Identification Toolbox is used to estimate the coefficients of a transfer function for this complex conjugate impedance matching controller, that will be referred to hereafter as the Feedback Resonating Controller (FBR). While enforcing stability, the FBR is determined by fitting a parametric model to the complex conjugate of the red curve in Fig. 2 over a limited frequency range.

The order of the FBR controller was determined by constraining it to be of similar order as the admittance model. For the device considered in this study, a second order model is used for both the impedance and the FBR because it provides the best trade-off between accuracy and simplicity. The resulting transfer function has the form

$$F_{PTO} = C(s) V = \frac{b_2 s^2 + b_1 s + b_0}{s^2 + a_1 s + a_0} V. \quad (9)$$

The general structure of a WEC with a reactive controller is shown in Fig. 3. The plant (oscillating body) is modeled as the inverse of the intrinsic impedance Z_i , where the input is force and the output is velocity; this model is also known as admittance model [24]. The exciting force applied by the waves are denoted by F_e and are considered as input disturbance. The controller is denoted by C whereas G is the dynamic model of the PTO, which is discussed in Section IV, and will be considered as $G = 1$ in the next section (Sec III). In this case, the closed loop transfer function between the excitation force F_e and the velocity response $V(s)$ is:

$$V = \frac{1}{Z_i(s) - C(s)} F_e. \quad (10)$$

III. RESULTS

The experimental data used in this paper were collected at the Naval Surface Warfare Center, Carderock Division Maneuvering and Sea Keeping (MASK) basin, on the single degree-of-freedom point-absorber device depicted in Fig. 1; details are provided in [24]. As described in the previous section, Fig. 2 shows the Bode plot of the device's parametric

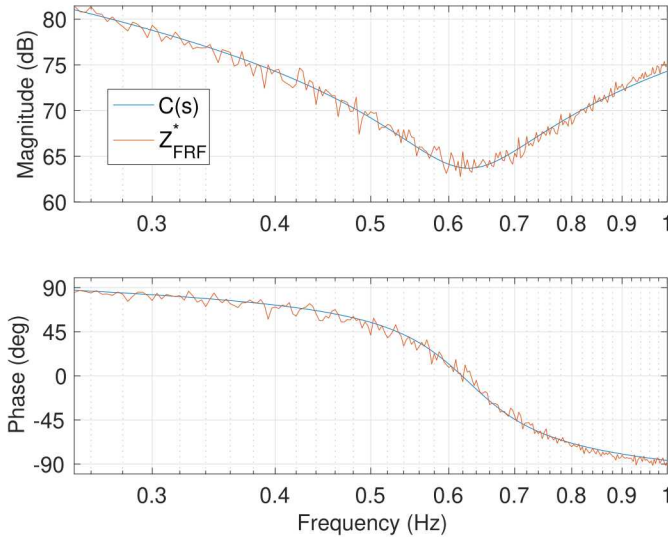


Fig. 4. Bode plot of the FBR controller $C(s)$ (blue curve) and non-parametric response used for SID (Z_{FRF}^* red curve).

and non-parametric models, whereas Fig. 4 shows the Bode plot of the non-parametric response (Z_{FRF}^*) of the optimal feedback (complex conjugate of the intrinsic impedance), and the identified FBR controller (blue line). It can be seen that the FBR controller is very close to the optimal over the frequency band $0.25 \leq f \leq 1$ Hz, in terms of both magnitude and phase. The scale of the device considered in this paper is assumed to be 1 : 17; therefore, at full scale, the frequency range corresponds to waves with periods between 4.1 s and 16.5 s, covering most of the sites where these devices could be potentially deployed. In other words, the choice of the frequency band is dependent on the site where the device will be deployed: the frequency range should be chosen so any excitation outside the chosen frequency range has a low probability of occurrence, therefore not affecting power production.

Figure 5 shows the pole-zero map of the FBR controller; it can be seen that the model is stable with all of the poles in the left hand side of the imaginary axis (negative real part). It is, however, non-minimum phase, as a pair of complex-conjugate zeros have a positive real part; although, there are no side effects. In fact, the resulting closed loop system in (10) is both stable and minimum phase, as shown in the pole-zero map in Fig. 6; all the poles and zeros lie on the left hand side of the imaginary axis. This is confirmed by the results plotted in Fig. 7, which shows the velocity response of a chirp input varying over a wide range of frequencies, in particular in the range of $0.0001 \leq f \leq 100$ Hz. The response of the chirp in Fig. 7, is also useful to see that the system resonates in the proximity of two different frequencies, at about 0.2 Hz and 1.1 Hz. As discussed above, these frequencies are outside the band of interest, and cause no harm, because the system is stable (all closed loop poles have negative real part).

Fig. 8 shows the power absorption efficiency of the FBR as a function of the frequency, which is calculated as the ratio between the average absorbed power when using the FBR

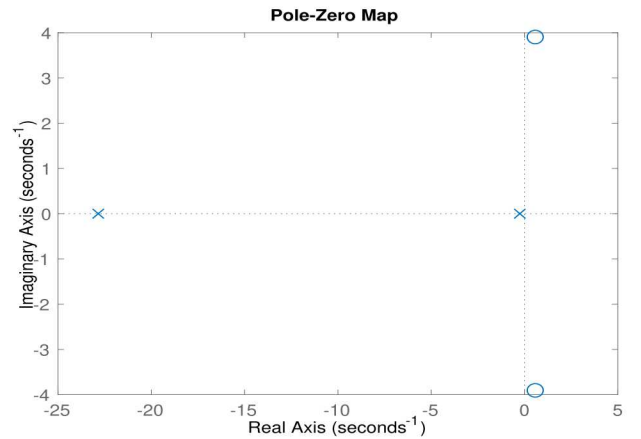


Fig. 5. Pole-zero map of FBR controller.

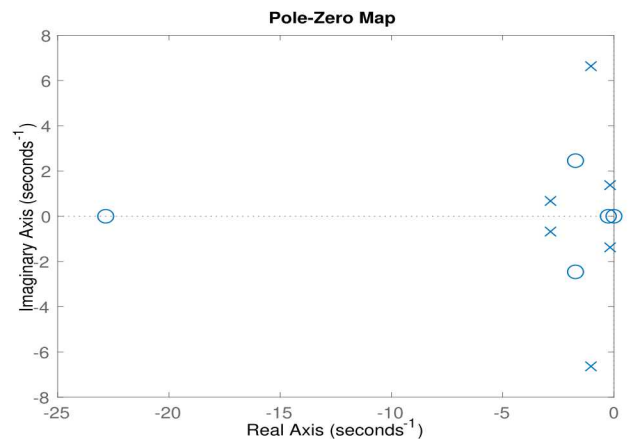


Fig. 6. Pole-zero map of closed loop system in (10).

and the theoretical maximum given by (7). Fig. 8 also shows normalized wave energy flux for three different sea states, listed in Table I. The wave energy flux J is the average power carried by waves per unit width of the wave front in deep water; the flux for each frequency component (J_i) is calculated as (see eq. 4.136 in [1]):

$$J_i = \frac{\rho g^2}{32\pi} T_i H_i^2, \quad (11)$$

where T_i is the period of the i -th frequency component of the wave ($T = 2\pi/\omega$) and H_i is the height of the i -th component. The total wave energy flux for each sea state is obtained by adding all the contributions from each frequency component, as $J = \sum_i J_i$. The H_i for each sea state are obtained as described in [29] (Sec. B.1), by assuming a JONSWAP spectral distribution [30] which is defined by three parameters: the peak period T_p , the significant wave height H_s , and the peak enhancement factor γ .

Table I shows the average power produced by FBR and CC controllers for individual sea states with the 1/17th-scale WEC. Note that although a single FBR controller could accommodate the full set of sea states shown in Table I, individual transfer functions were produced for each case. This approach reflects an understanding that the likely application of such a control system would involve gain scheduling based on the slowly

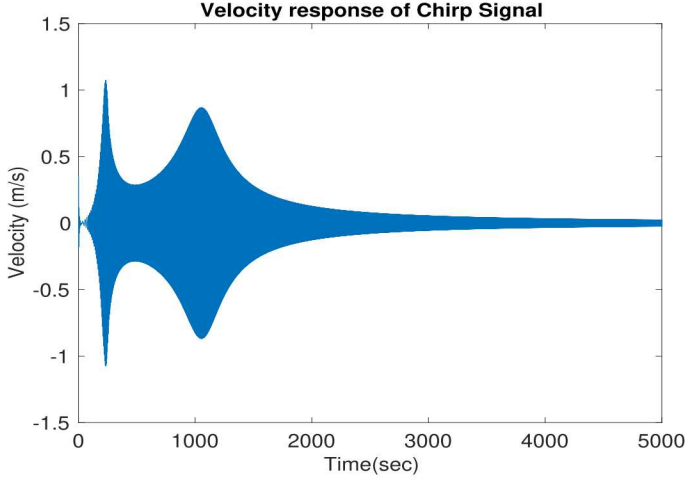


Fig. 7. Velocity response for chirp signal ranging from $0.0001 \leq f \leq 100$ Hz.

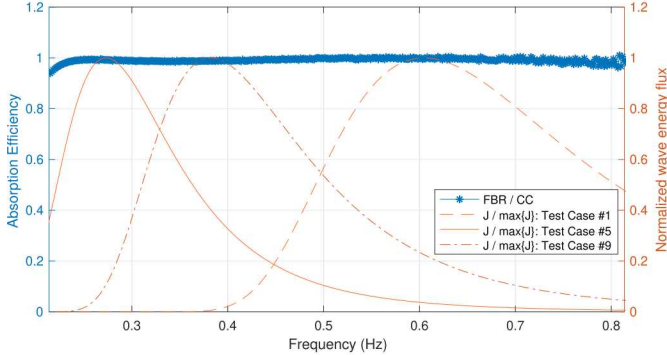


Fig. 8. Power absorption efficiency compared with the theoretical maximum.

changing sea state. With this approach, the FBR controller attains greater than 90% of the theoretical optimum across all of the sea states considered.

IV. PTO DYNAMICS

The control design approach presented in Section II and the results in Section III concern the maximization of the mechanical power at the interface between the PTO and the

TABLE I
POWER OUTPUT FOR MODEL-SCALE WEC WITH ACAUSAL COMPLEX-CONJUGATE (CC) AND FEEDBACK RESONATING (FBR) CONTROLLERS.

Test Case	T_p [s]	H_s [m]	γ	CC	FBR	FBR/CC
1	1.58	0.127	1	3.6	3.5	0.97
2	1.58	0.127	3.3	4	3.8	0.95
3	2.5	0.127	1	18.4	17.4	0.95
4	2.5	0.127	3.3	20.5	19.4	0.95
5	2.5	0.254	1	73.6	70	0.95
6	2.5	0.254	3.3	81.9	78	0.95
7	3.5	0.127	1	71	65.8	0.93
8	3.5	0.127	3.3	77.7	72.3	0.93
9	3.5	0.254	1	284.2	259.5	0.91
10	3.5	0.254	3.3	310.7	290.4	0.93
Mean				94.56	88.01	0.93

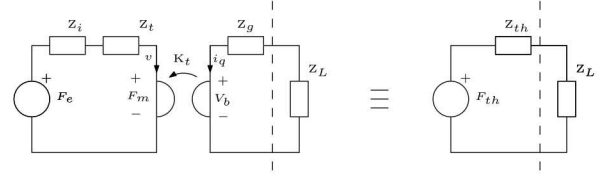


Fig. 9. WEC with direct drive PTO model and its Thévenin equivalent circuit.

oscillating buoy. This configuration and objective are the ones commonly considered in the literature, and also, for this reason, have been the main focus of this paper. However, in practice, the objective of the control system is to maximize the electrical power (or other form of useful power) provided to the end user—that is at output of the PTO. In this case, the control system design should be carried out by using the overall coupled dynamics of the buoy and the PTO.

The control design approach presented in Section II can still be used by redefining the intrinsic impedance of the device with an equivalent impedance by using a Thévenin equivalent circuit, as shown in Fig. 9 for the direct drive system used in the WaveBot device. The left hand side of Fig. 9 describes the WEC dynamics as an electrical equivalent, where $Z_t = R_t + iX_t$ denotes the drive-train impedance, which is composed of a resistive term (R_t) that models friction and a reactive term for inertia and compliance (X_t). The force applied by the motor is denoted by F_m , the quantity K_t is the motor constant, V_b is the back-EMF and Z_g is the winding impedance of the generator. The equivalent impedance Z_{th} is

$$Z_{th} = \left(\frac{K_t^2}{Z_d + Z_i} - Z_g \right). \quad (12)$$

The quadrature current i_q is the control variable; the controller can then be derived in the same manner by approximating the Thévenin equivalent impedance Z_{th} with a casual transfer function over a given frequency range.

V. CONCLUSIONS

This paper briefly described the non-casual issue of the reactive controller for a WEC, and introduced the use of SID methods to derive a stable and casual band-limited controller, the FBR controller. By inspection of the pole-zero map and by using a wide range chirp signal as the input, the stability of the closed loop response has been confirmed. The power captured efficiency of the controller was compared to the theoretical maximum power capture. The average power capture efficiency over the analyzed frequency band was found to be 99% of the theoretical maximum over the frequency range of interest.

From the above results, the FBR controller performs well within the frequency bands considered. Close to the edges of these frequency bands the efficiency in the SID model starts to decrease and the system can perform worse. To remedy this issue, future experimental testing could be performed for a broader frequency range, thus enabling the design of a broader banded FBR controller. On the other hand, if the experimental model is considered to be at a 1 : 17 scale, the frequency range

of $0.25 \leq f \leq 0.1$ Hz corresponds to waves with periods between 4.1 s and 16.5 s at full scale, which could be entirely sufficient to cover many of the wave sites where these devices will likely to be located.

REFERENCES

- [1] J. Falnes, *Ocean Waves and Oscillating Systems*. Cambridge; New York: Cambridge University Press, 2002.
- [2] —, “Optimum control of oscillation of wave-energy converters,” vol. 12, 06 2002.
- [3] —, “Principles for capture of energy from ocean waves: phase control and optimum oscillation,” 1997. [Online]. Available: http://folk.ntnu.no/falnes/web_arkiv/InstFysikk/phcontrl.pdf
- [4] U. Korde, “Control system applications in wave energy conversion,” in *OCEANS 2000 MTS/IEEE Conference and Exhibition*, vol. 3, 2000, pp. 1817–1824 vol.3.
- [5] R. G. Coe, G. Bacelli, D. G. Wilson, O. Abdelkhalik, U. A. Korde, and R. D. R. III, “A comparison of control strategies for wave energy converters,” *International Journal of Marine Energy*, vol. 20, no. Supplement C, pp. 45 – 63, 2017. [Online]. Available: <http://www.sciencedirect.com/science/article/pii/S2214166917300905>
- [6] U. Korde, “On providing a reaction for efficient wave energy absorption by floating devices,” *Applied Ocean Research*, vol. 21, no. 5, pp. 235 – 248, 1999. [Online]. Available: <http://www.sciencedirect.com/science/article/pii/S0141118799000097>
- [7] U. A. Korde, “Systems of reactively loaded coupled oscillating bodies in wave energy conversion,” *Applied Ocean Research*, vol. 25, no. 2, pp. 79 – 91, 2003. [Online]. Available: <http://www.sciencedirect.com/science/article/pii/S0141118703000440>
- [8] J. Falnes, “Wave-energy conversion through relative motion between two single-mode oscillating bodies,” *Journal of Offshore Mechanics and Arctic Engineering*, vol. 121, no. 1, pp. 32–38, Feb. 1999. [Online]. Available: <http://dx.doi.org/10.1115/1.2829552>
- [9] J. Falnes *et al.*, “Optimum control of oscillation of wave-energy converters,” *International Journal of Offshore and Polar Engineering*, vol. 12, no. 02, 2002.
- [10] A. F. d. O. Falcao and P. A. P. Justino, “OWC wave energy devices with air flow control,” *Ocean Engineering*, vol. 26, no. 12, pp. 1275–1295, Dec. 1999. [Online]. Available: <http://www.sciencedirect.com/science/article/pii/S0029801898000754>
- [11] J. Hals, J. Falnes, and T. Moan, “Constrained optimal control of a heaving buoy wave-energy converter,” *Journal of Offshore Mechanics and Arctic Engineering*, vol. 133, no. 1, pp. 1–15, 2011.
- [12] G. Bacelli, R. Genest, and J. V. Ringwood, “Nonlinear control of flap-type wave energy converter with a non-ideal power take-off system,” *Annual Reviews in Control*, vol. 40, pp. 116–126, 2015.
- [13] R. G. Coe, G. Bacelli, D. Patterson, and D. G. Wilson, “Advanced WEC Dynamics & Controls FY16 testing report,” Sandia National Labs, Albuquerque, NM, Tech. Rep. SAND2016-10094, October 2016. [Online]. Available: <https://mhkdr.openei.org/submissions/151>
- [14] E. Tedeschi, M. Molinas, M. Carraro, and P. Mattavelli, “Analysis of power extraction from irregular waves by all-electric power take off,” in *2010 IEEE Energy Conversion Congress and Exposition*, Sept 2010, pp. 2370–2377.
- [15] E. Tedeschi, M. Carraro, M. Molinas, and P. Mattavelli, “Effect of control strategies and power take-off efficiency on the power capture from sea waves,” *IEEE Transactions on Energy Conversion*, vol. 26, no. 4, pp. 1088–1098, Dec 2011.
- [16] H. Yavuz, S. Mısıkoğlu, and T. Stallard, “Processing irregular wave measurements to enhance point absorber power capture performance,” *Ocean Engineering*, vol. 38, no. 4, pp. 684 – 698, 2011. [Online]. Available: <http://www.sciencedirect.com/science/article/pii/S0029801810002866>
- [17] F. Fusco and J. Ringwood, “A model for the sensitivity of non-causal control of wave energy converters to wave excitation force prediction errors,” *Proceedings of the 9th European Wave and Tidal Energy Conference (EWTEC)*, September 2011. [Online]. Available: <http://eprints.maynoothuniversity.ie/3551/>
- [18] —, “Quantification of the prediction requirements in reactive control of wave energy converters,” *IFAC Proceedings Volumes*, vol. 44, no. 1, pp. 11483 – 11488, 2011, 18th IFAC World Congress. [Online]. Available: <http://www.sciencedirect.com/science/article/pii/S1474667016454601>
- [19] F. Fusco and J. V. Ringwood, “A study of the prediction requirements in real-time control of wave energy converters,” *IEEE Transactions on Sustainable Energy*, vol. 3, no. 1, pp. 176–184, Jan 2012.
- [20] E. Anderlini, D. Forehand, E. Bannon, and M. Abusara, “Reactive control of a wave energy converter using artificial neural networks,” *International Journal of Marine Energy*, vol. 19, no. Supplement C, pp. 207 – 220, 2017. [Online]. Available: <http://www.sciencedirect.com/science/article/pii/S2214166917300668>
- [21] E. Anderlini, D. Forehand, E. Bannon, Q. Xiao, and M. Abusara, “Reactive control of a two-body point absorber using reinforcement learning,” *Ocean Engineering*, 2017. [Online]. Available: <http://www.sciencedirect.com/science/article/pii/S0029801817304699>
- [22] S. R. Nielsen, Q. Zhou, M. M. Kramer, B. Basu, and Z. Zhang, “Optimal control of nonlinear wave energy point converters,” *Ocean Engineering*, vol. 72, no. Supplement C, pp. 176 – 187, 2013. [Online]. Available: <http://www.sciencedirect.com/science/article/pii/S0029801813002758>
- [23] V. Nevarez, G. Bacelli, R. G. Coe, and D. G. Wilson, “Feedback resonating control for a wave energy converter,” in *Proceedings of SPEEDAM2018*, 2018.
- [24] G. Bacelli, R. G. Coe, D. Patterson, and D. Wilson, “System identification of a heaving point absorber: Design of experiment and device modeling,” *Energies*, vol. 10, no. 10, p. 472, 2017. [Online]. Available: <http://www.mdpi.com/1996-1073/10/4/472>
- [25] S. Giorgi, J. Davidson, and J. V. Ringwood, “Identification of wave energy device models from numerical wave tank data part 2: Data-based model determination,” *IEEE Transactions on Sustainable Energy*, vol. 7, no. 3, pp. 1020–1027, July 2016.
- [26] H. Cho, G. Bacelli, and R. G. Coe, “Linear and nonlinear system identification of a wave energy converter,” in *Proceedings of the 6th Marine Energy Technology Symposium (METS)*, Washington, D.C., 2018.
- [27] H. W. Bode, *Network Analysis and Feedback Amplifier Design*. New York: Van Nostrand, 1945.
- [28] R. M. Fano, “Theoretical limitations on the broadband matching of arbitrary impedances,” *Journal of the Franklin Institute*, vol. 249, no. 1, pp. 57 – 83, 1950. [Online]. Available: <http://www.sciencedirect.com/science/article/pii/0016003250900068>
- [29] WAFO-group, *WAFO - A Matlab Toolbox for Analysis of Random Waves and Loads - A Tutorial*, Math. Stat., Center for Math. Sci., Lund Univ., Lund, Sweden. [Online]. Available: <http://www.maths.lth.se/matstat/wafo>
- [30] K. Hasselmann, T. Barnett, E. Bouws, H. Carlson, D. Cartwright, K. Enke, J. Ewing, H. Gienapp, D. Hasselmann, P. Kruseman *et al.*, “Measurements of wind-wave growth and swell decay during the joint north sea wave project (JONSWAP),” *Ergänzungsheft 8-12*, 1973.